

Diagnostics of ionized gas in galaxies with the “BPT–radial velocity dispersion” relation

D.V. Oparin^{1*} and A.V. Moiseev^{2***}

¹Special Astrophysical Observatory, Russian Academy of Sciences, Nizhnij Arkhyz, 369167 Russia

²S2Space Research Institute, Moscow, 117997 Russia

March 30, 2018/Revised: June 28, 2018

Abstract. In order to study the state of gas in galaxies, diagrams of the relation of optical emission line fluxes are used allowing one to separate main ionization sources: young stars in the H II regions, active galactic nuclei, and shock waves. In the intermediate cases, when the contributions of radiation from OB stars and from shock waves mix, identification becomes uncertain, and the issue remains unresolved on what determines the observed state of the diffuse ionized gas (DIG) including the one on large distances from the galactic plane. Adding of an extra parameter — the gas line-of-sight velocity dispersion — to classical diagnostic diagrams helps to find a solution. In the present paper, we analyze the observed data for several nearby galaxies: for UGC 10043 with the galactic wind, for the star forming dwarf galaxies VII Zw 403 and Mrk 35, for the galaxy Arp 212 with a polar ring. The data on the velocity dispersion are obtained at the 6-m SAO RAS telescope with the Fabry-Perot scanning interferometer, the information on the relation of main emission-line fluxes — from the published results of the integral-field spectroscopy (the CALIFA survey and the MPFS spectrograph). A positive correlation between the radial velocity dispersion and the contribution of shock excitation to gas ionization are observed. In particular, in studying Arp 212, “BPT– σ relation” allowed us to confirm the assumption on a direct collision of gaseous clouds on the inclined orbits with the main disk of the galaxy.

Key words. galaxies: interstellar medium—galaxies: kinematics and dynamics—galaxies: star formation

1. Introduction

Diagrams of ratios of optical emission-line fluxes are widely used for diagnostics of gas-ionization sources in galaxies. In the classic work by Baldwin, Phillips, & Terlevich (1981) the two-dimension diagram of line fluxes of $[\text{O III}]\lambda 5007/\text{H}\beta$ and $[\text{N II}]\lambda 6583/\text{H}\alpha$ was suggested for separation of objects with different ionization sources. The method became popular due to the use of measurements of lines bright in the visible range that are close in wavelengths and, consequently, with a weak dependence of their intensity ratio on the interstellar extinction. Later, this method was extended by adding the relations $[\text{S II}]/\text{H}\alpha$ ¹ and $[\text{O I}]/\text{H}\alpha$ (Veilleux & Osterbrock, 1987; Kewley et al., 2001) as the second parameter. All the mentioned diagrams are frequently called in the literature the “BPT diagrams” after the authors of the method. Using them, it is possible to distinguish the regions, where the largest

contribution to gas ionization is made by young massive stars (hereinafter, the H II type) and the regions of dominating hard ionizing radiation of the active galactic nucleus (AGN). At the same time, the regions ionized by shock waves, the asymptotic giant branch (AGB) stars or nuclei of galaxies of the LINER type mix in the diagrams². Various variants of the demarcation lines were suggested (Monreal-Ibero et al., 2010; Ho et al., 2014), but it is often problematic to separate the contribution of ionizing sources with the soft spectrum.

Addition of one more parameter – the velocity dispersion of the ionized gas along the line of sight (σ) – to the classic diagnostic diagrams allows one to escape uncertainty in the cases, when the increase of σ indicates the increase of turbulent velocities of gas beyond the front of a shock wave. However, to estimate σ reliably, the spectral resolution is necessary that is noticeably better than that usually required for measuring the fluxes of radial velocities of separate spectral lines. Thus, until recently, the dependence of the relation of line fluxes characteriz-

Send offprint requests to: Dmitry Oparin e-mail: doparin2@gmail.com

¹ Hereinafter, for short we will designate $[\text{O I}]\lambda 6300$ as $[\text{O I}]$, $[\text{O III}]\lambda 5007$ as $[\text{O III}]$, $[\text{N II}]\lambda 6583$ as $[\text{N II}]$, and $[\text{S II}]\lambda 6717+[\text{S II}]\lambda 6731$ as $[\text{S II}]$.

² Low-Ionization Narrow Emission-line Region in which the shock ionization of gas can be associated both with a burst of star formation and with a weak nuclear activity.

ing the shock ionization from σ was rarely considered and mainly for the objects with $\sigma > 100\text{--}200 \text{ km s}^{-1}$ such as galaxies with intense star formation (Monreal-Ibero et al., 2010; Ho et al., 2014). Such an approach has not previously been used to study the ionization of diffuse gas in dwarf galaxies, around separate star-forming regions, or at some distance from the plane of the galactic disk.

There is a discussion about the sources of ionization of this diffuse ionized gas (DIG) in galaxies whose role is assigned to an old stellar population, leakage of Lyman quanta from H II regions, and also possibly to shock fronts caused by star formation processes (see references and discussion in Jones et al., 2017; Egorov et al., 2017). The most effective methods for studying the extended low-brightness structures in galaxies are panoramic spectroscopy also called integral-field, or 3D. In a recent paper based on the results of the SDSS MaNGA survey by (Zhang et al., 2017), it was concluded that DIG is associated mainly with the evolved stellar population (AGB stars, etc.). At the same time, in Section 6.2 of the paper cited, it was noted that shock waves can be the cause of the observed increase in the flux ratio of the forbidden and Balmer lines. It is difficult to verify, since the spectral resolution of the MaNGA survey is about two times poorer than that required to be able see the effects of moderate shock waves (with a velocity of less than 500 km s^{-1}) in the observed kinematics of the ionized gas. Unfortunately, most of the available observed data on spectrophotometry and kinematics of the gas of nearby galaxies are obtained with the spectral resolution $FWHM > 5 \text{ \AA}$ which corresponds to values greater than 100 km s^{-1} in terms of radial velocity dispersion or greater than 230 km s^{-1} in terms of the $FWHM$ in the H α line. Observations with such resolution are a compulsory compromise in the study of low-surface-brightness objects.

In the SAMI survey of galaxies (Ho et al., 2014) with the 3D spectroscopy at the 3.9-m Anglo-Australian Telescope (AAT), the “line ratio–velocity dispersion” diagrams were built for the galaxies with active star formation. A positive correlation of the ionized gas σ with a characteristic emission lines ratios was noticed, which was interpreted as an increase of shock waves contribution with velocities of about $200\text{--}300 \text{ km s}^{-1}$ accompanying a burst of star formation. The spectral resolution of the SAMI survey is greater than that of MaNGA and equals $R \approx 4500$.

A significant limitation of these two most massive today 3D spectroscopy surveys of galaxies is rather low spatial resolution (more than 1 kpc). It is related to the fact that the field of view of integral field unit (IFU) is small and is about $15''$ in SAMI (Croom et al., 2012) and $12''\text{--}32''$ in SDSS MaNGA (Bundy et al., 2015). In these surveys, relatively distant ($z > 0.01$) galaxies are studied. At the same time, the largest contribution to the kinematics of interstellar medium from motion due to supernovae and winds of young stars in star-forming regions is made on considerably smaller spatial scales (from tens to hundreds of parsec). Consequently, any observed manifesta-

tions of shock fronts in star-forming regions become unev-ident, when averaging over a scale of one kpc or more. The examples of decreasing of peak velocity dispersion of the ionized gas in dwarf galaxies with degradation of a spatial resolution are presented in Moiseev & Lozinskaya (2012). Vasiliev et al. (2015) considered the same effect in simulations of multiple supernova explosions. Therefore, for observational studies of the relation between an ionization state of gas and dispersion of its radial velocities in galaxies without an active nucleus and with a moderate star formation rate, 3D spectroscopic data are required simultaneously with a considerably high spectral and spatial resolution.

In this paper, we consider this relation for several nearby galaxies using a combination of two spectroscopic methods with similar spatial resolution and quite a large field of view. Velocity dispersion map are derived from the observations with a scanning Fabry-Perot interferometer (FPI) at the 6-m SAO RAS telescope. Information on the main emission lines ratios are taken from open data on the integral-field spectroscopy with low spectral resolution.

In order to show the relation between the velocity dispersion and the lines ratios characterizing the ionization state, we use various methods through our paper: coloring in BPT diagrams, the “ σ –line-flux relation” diagrams, and “ σ –distance from the H II/AGN demarcation line.” *As a general name for the dependencies under study, we use the term “BPT relation– σ ”.* Classical BPT–diagrams are two-dimensional plots, where the axes represent relations of line fluxes. The inclusion of the velocity dispersion in the analysis is equivalent to the transition to three-dimensional plots, where a coordinate axis σ is added to each diagram. The more familiar two-dimensional plots given in our paper and in the above papers are a projection of the BPT– σ common relation to the selected plane.

2. Spectral data and data reduction

2.1. Galaxy Sample

We considered the sample of galaxies with data on a ionized gas state obtained with two 3D spectroscopy methods. When compiling the sample, we prepared a list of nearby galaxies for which, based on observations with the scanning FPI at the 6-m telescope of SAO RAS, the fields of velocity dispersion of ionized gas in the H α or [N II] emission lines were constructed. In total, this is about 60 objects that were observed in 2002–2015; most of them are presented in Moiseev et al. (2015). For each galaxy in the list, we checked the presence of data cubes in open sources obtained with the integral-field spectroscopy. For three galaxies: Arp 212, Mrk 35, and UGC 10043 such data were obtained within the framework of the CALIFA survey (The Calar-Alto Legacy Integral Field Area, Sánchez et al., 2011). We used the third data release of CALIFA; the spectra are available on the project website³. Let us

³ <http://califa.caha.es/>

Table 1. Characteristics of the galaxies under study and parameters of their observations with different methods

Galaxy	D , Mpc	M_B	Integral-field spectroscopy				Scanning FPI		
			Instrument	$\Delta\lambda$, Å	$\delta\lambda$, Å	θ''	$\Delta\lambda$	$\delta\lambda$, Å	θ''
UGC 10043	34.9	-17.6	PPAK	3750–7500	5–9	2.7	[N II]	1.7	1.5
VII Zw 403 (UGC 6456)	4.34	-13.87	MPFS	4250–7200	8	2.0	H α	0.8	2.2
Mrk 35 (NGC 3353)	15.6	-17.75	PPAK	3750–7500	5–9	2.7	H α	0.8	2.1
Arp 212 (NGC 7625)	23.5	-18.9	PPAK	3750–7500	5–9	2.7	H α	0.8	2.7

notice that UGC 10043 was observed with the 6-m telescope specially on request of the CALIFA team. The results were presented in our collaborative paper (López-Cobá et al., 2017) and triggered our interest for further study of the BPT- σ relation. Nevertheless, to keep homogeneity, we repeated the analysis of the UGC 10043 data in this paper using the same methods as for other galaxies. For the galaxy VII Zw 403, there was a data cube obtained by combining several fields of the MPFS spectrograph in observations at the 6-m telescope of SAO RAS and published by Arkhipova et al. (2007).

Table 1 briefly presents the objects under study (accepted distance D and absolute magnitude M_B based on the NED data) and on the data used (observation instruments, $\Delta\lambda$ -spectral range or a selected line, $\delta\lambda$ -spectral resolution in terms of $FWHM$, θ'' -angular resolution). Figure 1 shows the images of the sample galaxies in the r filter and in the emission lines, and velocity dispersion fields σ of the ionized gas constructed from the scanning FPI data. It also shows the field of view of the spectrographs used.

2.2. Low-Resolution Spectra

For UGC 10043, Mrk 35, and Arp 212, we used the CALIFA data obtained at the 3.5-m telescope of the Calar Alto observatory in the mode of the integral-field spectroscopy of the PPAK wide field (Kelz et al., 2006) of the PMAS spectrograph (Roth et al., 2005). The array of PPAK optical fibers comprises 331 elements of the 2'' diameter collected in the 74'' \times 64'' hexagonal field. We used the cubes obtained in the low-resolution mode covering the entire visible range (grating V500, $R \sim 850$). The reduced data are presented in the form of cubes extrapolated from a hexagonal grid to a square grid with a spatial element size (spaxel) of 1''.

The galaxy VII Zw 403 was observed with the MPFS multislit spectrograph (Afanasiev et al., 2001) at the SAO RAS 6-m telescope. An array of square lenses combined with fiber optics provided a field of view of 16 \times 16 elements with a scale of 1'' per lens. The data cube presented in Arkhipova et al. (2007) is a mosaic of the size of 49'' \times 31'' comprising seven MPFS fields. The spectral range was 4250–7200 Å; the resolution was 8 Å.

For the analysis, we used the data cubes with the 2 \times 2 binning to a scale of 2'' per element (see next Section 2.3). Approximation of the lines in the spectra was carried out by the one-component Gaussian function. The line

fluxes ratios were measured only from the spectra in which $S/N > 2$ for each emission line. The local continuum level near each line was taken into account.

2.3. Kinematics of the Ionized Gas

The archival observations with the scanning Fabry-Perot interferometer installed at the SCORPIO (Afanasiev & Moiseev, 2005) and SCORPIO-2 (Afanasiev & Moiseev, 2011) focal reducers in the primary focus of the 6-m telescope were used to create the velocity dispersion maps. The emission line (H α or [N II] λ 6583) was selected with the a narrow-band filter with a bandwidth $\sim 20\text{Å}$. UGC 10043 was observed with the IFP186 interferometer providing the spectral resolution $FWHM = 1.7\text{Å}$. In the study of other galaxies, IFP501 with the resolution $FWHM = 0.8\text{Å}$ was used. In observations of VII Zw 403, the image scale was 0''.56 px $^{-1}$ with the field of view of 4'.8, for other galaxies: 0''.7 px $^{-1}$ and 6'.1, respectively. The result of the reduction of the set of interferograms was a data cube, where each pixel contained the spectrum of the selected emission line consisting of 36–40 channels. The details of data reduction and observational logs were published earlier (see references in Section 3). Since the instrumental contour of the interferometer is well described with the Lorentz profile, the observed profiles of emission lines were approximated by the Voigt function — the convolution of the Gauss and Lorentz functions (Moiseev & Egorov, 2008). It is assumed that the initial (without any instrumental broadening) profile of an emission line is satisfactorily described by a Gaussian, which is a good approximation for observations of H II regions, with the exception of individual peculiar cases (expanding envelopes, neighborhood of Wolf-Rayet stars, etc. (see Moiseev & Lozinskaya, 2012; Egorov et al., 2017)). Based on the results of approximation, we built the monochromatic images in this line, the distribution of radial velocities of the ionized gas, and the radial velocity dispersion maps free from the instrumental broadening of the spectral line profile (Moiseev & Egorov, 2008).

The σ maps in Fig. 1 are shown with the original sampling of the FPI images (0''.6–0''.7) which is better than in the data used in the integral-field spectroscopy (1''/spaxel), while the angular resolution θ of both data sets is similar (see Table 1). To account for this effect, first we interpolated the FPI cube to a coarser grid corresponding to the CALIFA or MPFS data. The accuracy of coincidence of both data sets was controlled from the

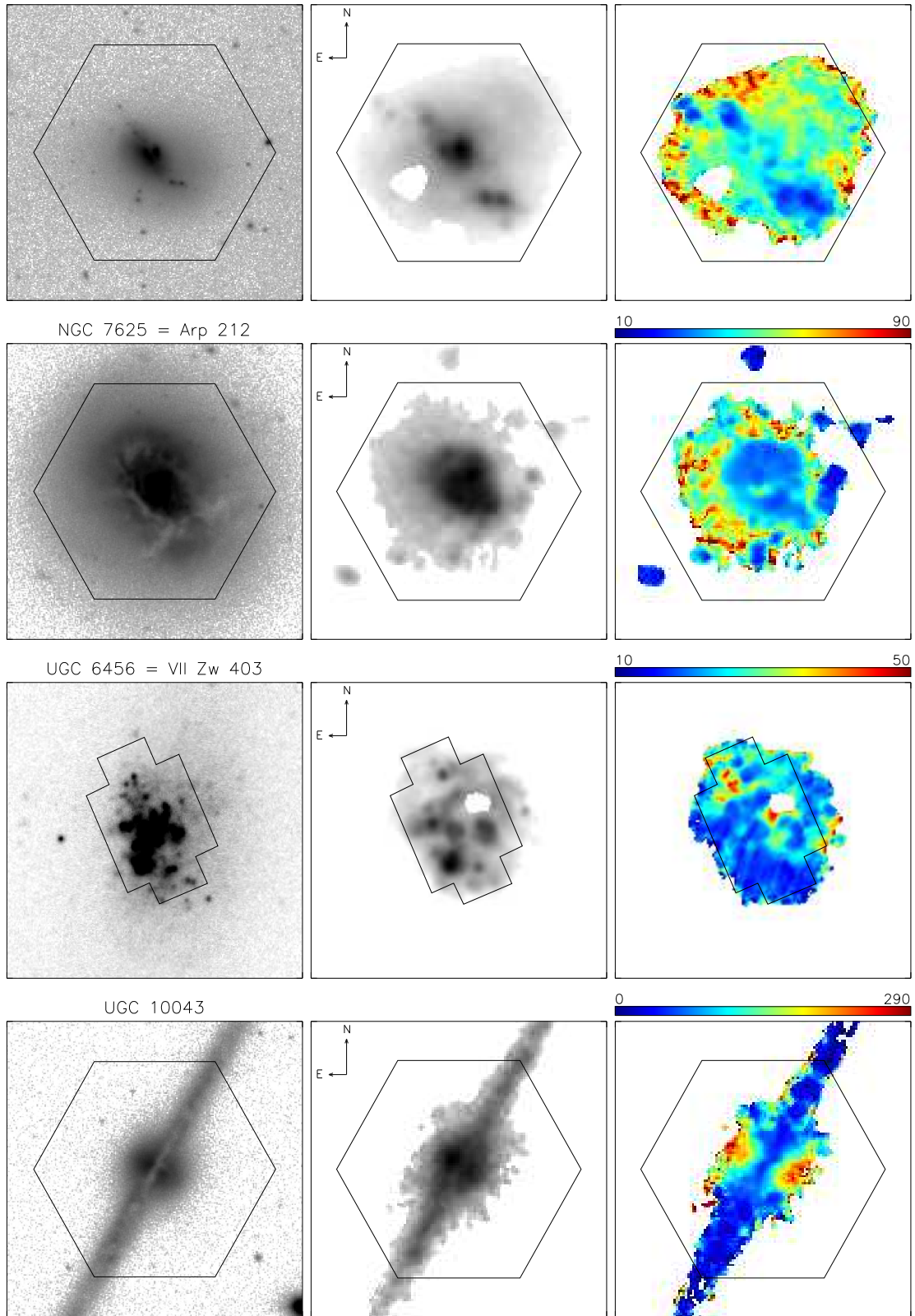


Fig. 1. The images of the studied galaxies. The left-hand column shows the SDSS r -filter images from Knapen et al. (2014), for UGC 6456 the image in the R filter is given from Gil de Paz et al. (2003). The middle column gives the images in the $[\text{N II}]\lambda 6583$ line (UGC 10043) or $\text{H}\alpha$ line (for others) from the observed data with the FPI at the 6-m BTA telescope. The right-hand column shows the velocity dispersion of the ionized gas; the scale in km s^{-1} . Image size is $90'' \times 90''$. The arrangement of the fields of view of integral-field spectrographs is shown: the CALIFA survey and the MPFS mosaic (for UGC 6456). The velocity dispersion fields are taken from Moiseev et al. (2015) and López-Cobá et al. (2017) (for UGC 10043) without correction for the thermal line broadening.

images in the emission lines and continuum and was better than $0''.2$ – $0''.5$. In order to detect the emission lines in the low-surface-brightness regions in the optimum way, we performed the pixel binning of 2×2 for both combined data sets. This procedure also reduced possible errors of a small difference between the angular resolution of the FPI data and integral-field spectroscopy. Therefore, all the measurements presented below are performed from the cubes with the $2''$ element size. After combining and binning in the FPI cubes, we built the maps σ . In the next section, these maps were used for direct per-pixel comparison with the low-resolution spectra.

We used masking to highlight the points with the ratio $S/N \geq 3$ in the maps σ . Let us note that, as distinct from Moiseev et al. (2015), we did not correct the velocity dispersion maps for thermal line broadening.

3. BPT– σ diagrams

3.1. Galactic Wind in UGC 10043

UGC 10043 is an edge-on spiral galaxy. Observations in the $H\alpha$ and $[\text{N II}]$ lines carried out with the HST (Matthews & de Grijs, 2004) have shown signs of star formation in the galactic core, as well as an extended emission structure that is perpendicular to the disk and is the result of the galactic wind influence. López-Cobá et al. (2017) presented diagnostic diagrams for the central part of the galaxy according to the CALIFA survey. Some of the points on the diagram relating to the central region of star formation turned out to be located in the region characteristic of photoionization by young stars, while others fell into the region typical of shock excitation. Within the framework of a shock excitation model, a wind velocity was constrained: no greater than 400 km s^{-1} . Analyzing the gas velocity field in the $[\text{N II}]$ line constructed with a scanning FPI allowed us to obtain a more strict limitation on the galactic wind velocity: less than 250 km s^{-1} in accordance with the gas shock excitation model. In the same paper López-Cobá et al. (2017), it has been shown that there is a distinct relation BPT– σ in the wind nebula of UGC 10043.

As it is shown in the diagnostic diagrams presented in Fig. 2 (the upper row), the regions with shock excitation of emission lines in the wind nebula are characterized by a higher velocity dispersion as compared to the regions dominated by photoionization. In this case, there is a positive correlation between the relations of line fluxes of $[\text{S II}]$ to $H\alpha$, of $[\text{N II}]$ to $H\alpha$, of $[\text{O I}]$ to $H\alpha$ and σ (see Fig. 2). At the same time, negative correlation is observed between the ratio of the sulfur doublet lines ($[\text{S II}]6731/[\text{S II}]6717$) and σ . This means that a higher velocity dispersion is characteristic of the diffuse gas with a lower electron density n_e .

We tried to quantify the BPT– σ relation. For each point in the diagrams of the lines ratios, it is possible to determine the minimum distance to the curve that bounds the H II-type ionization region from Kewley et al. (2001)

(in the case of the $[\text{N II}]/H\alpha$ – $[\text{O III}]/H\beta$ diagram, this is the boundary between the Comp and AGN regions in our figures). We marked this distance as ρ and determined it so that negative values of ρ corresponded to the shift of the points from the demarcation line to the side corresponding to photoionization by young stars, and positive–towards other ionization mechanisms. Figure 3 shows the examples of relations involved this parameter. For brevity and convenience of reading, we have designated the value ρ for the $[\text{N II}]/H\alpha$ – $[\text{O III}]/H\beta$ diagrams as $\rho([\text{N II}])$, for the $[\text{S II}]/H\alpha$ – $[\text{O III}]/H\beta$ diagrams as $\rho([\text{S II}])$, and for the $[\text{O I}]/H\alpha$ – $[\text{O III}]/H\beta$ diagrams as $\rho([\text{O I}])$. It can be seen that in all the cases presented, the increase in the velocity dispersion along the line of sight correlates with the distance from the region characteristic of ionization by young stars in the BPT diagram.

3.2. Mrk 35 and VII Zw 403—Dwarf Galaxies with a Burst of Star Formation

VII Zw 403 is one of the nearest blue compact dwarf galaxies with several episodes of recent star formation. The current outburst is located in the central kpc, where several compact OB-stars associations are identified and the associated H II shells that are immersed in the diffuse ionized gas (see Egorov & Lozinskaya, 2011, and references therein). The fields of velocities and velocity dispersions of the ionized gas in this galaxy were previously considered in Lozinskaya et al. (2006); Moiseev & Lozinskaya (2012); Moiseev et al. (2015), where a sufficiently quiet kinematics of the gas with a low level of peculiar velocities was noticed. The value σ is in the range of 15 – 40 km s^{-1} . In the BPT diagrams, most points are located in the region of photoionization (see Fig. 4). A certain number of points with higher dispersion are found near the separation curve. Along with this, the expanding H II shells associated with bright star formation regions are characterized by a smaller value of $\sigma \sim 20 \text{ km s}^{-1}$. One of the regions with a higher σ is located between these two shells. Others are located on the periphery of the ionized gas disk (Moiseev & Lozinskaya, 2012). In the “lines ratio–velocity dispersion” diagrams, there are no noticeably significant correlations (Fig. 4). Therefore, we can conclude that the contribution of shock excitation to gas ionization in this galaxy is negligible and even at the boundaries of the expanding shells it is noticeably inferior to photoionization (the H II type). This is also indicated by the absence of significant correlation between ρ and σ in Fig. 5.

Mrk 35 is another example of a blue compact galaxy. The ongoing star formation here is concentrated in several bright compact regions. Star-forming regions near the optical center of the galaxy form a bar-like structure, where the population of Wolf–Rayet stars is observed (Cairós et al., 2007). The radial velocity dispersion of the ionized gas in the galaxy reaches about 70 km s^{-1} , whereas in the central regions it lies within the range of 20 – 35 km s^{-1} . The highest dispersion of radial velocities is observed in

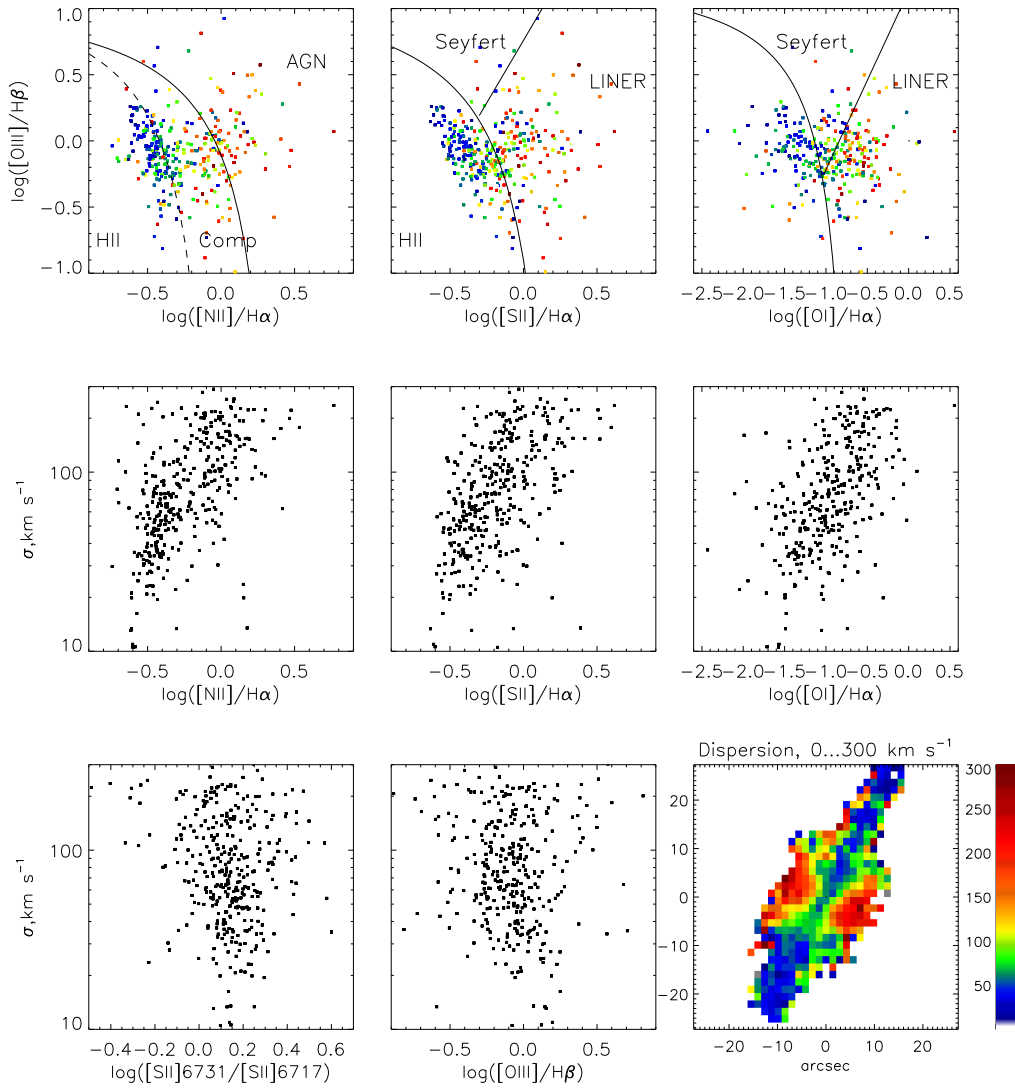


Fig. 2. Upper row: BPT diagrams for UGC 10043. The ionized gas line-of-sight velocity dispersion in the given pixel according to the map shown bottom right is colored. The lines separating the H II regions, the objects with the combined ionization type active Seyfert galaxies, and LINER are taken from Kewley et al. (2006). The other diagrams: the dependence between the velocity dispersion and the emission lines ratios

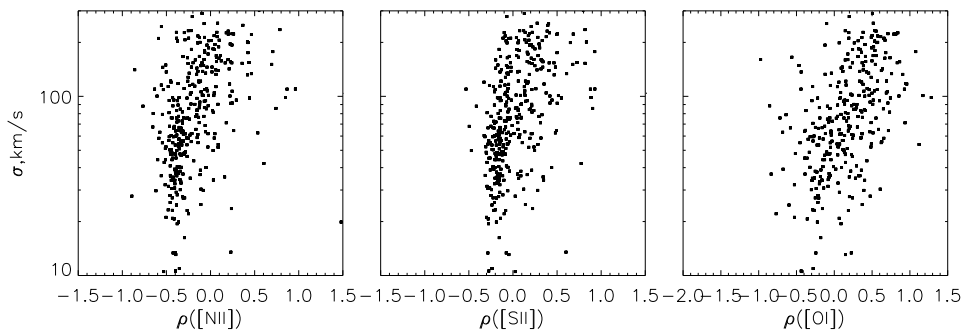


Fig. 3. UGC 10043. Dependence of σ on the distance of the point to the demarcation curve in the BPT diagram separating the H II regions and regions with other ionization mechanisms (according Kewley et al., 2001).

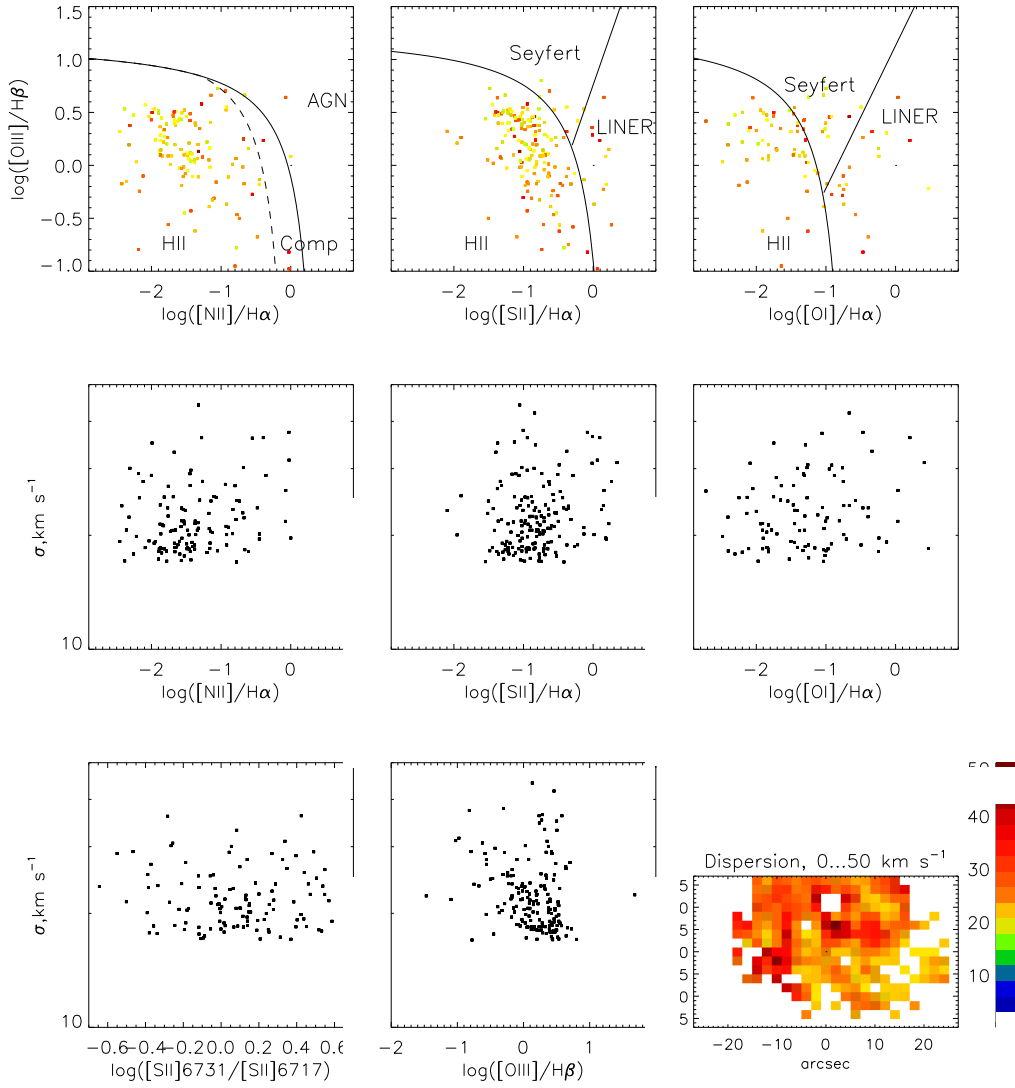


Fig. 4. Same as in Fig. 2, for VII Zw 403.

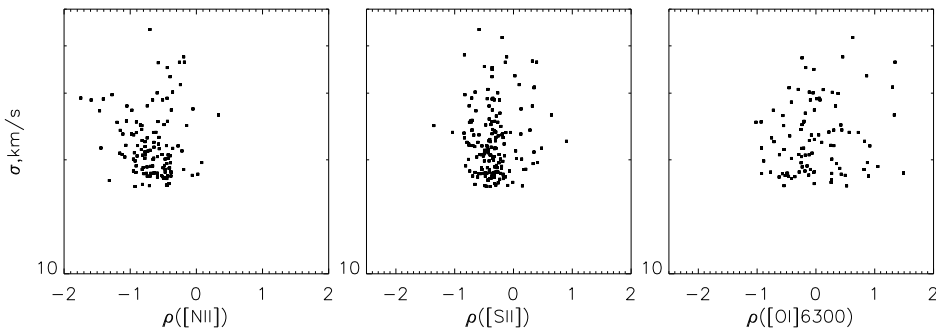


Fig. 5. Diagrams similar to those in Fig. 3, for VII Zw 403.

the gas located between three central regions of star formation. In the “arms”, the dispersion is several times lower in comparison with the central regions; and as a whole does not exceed 20 km s^{-1} . In the BPT diagrams (see Fig. 6), the points corresponding to the regions with

the ongoing star formation are located in the region of photoionization. The outer parts of the galaxy, characterized by low surface brightness and high dispersion of radial velocities, appear near the separation curves which suggests a certain contribution of shock waves to the gas

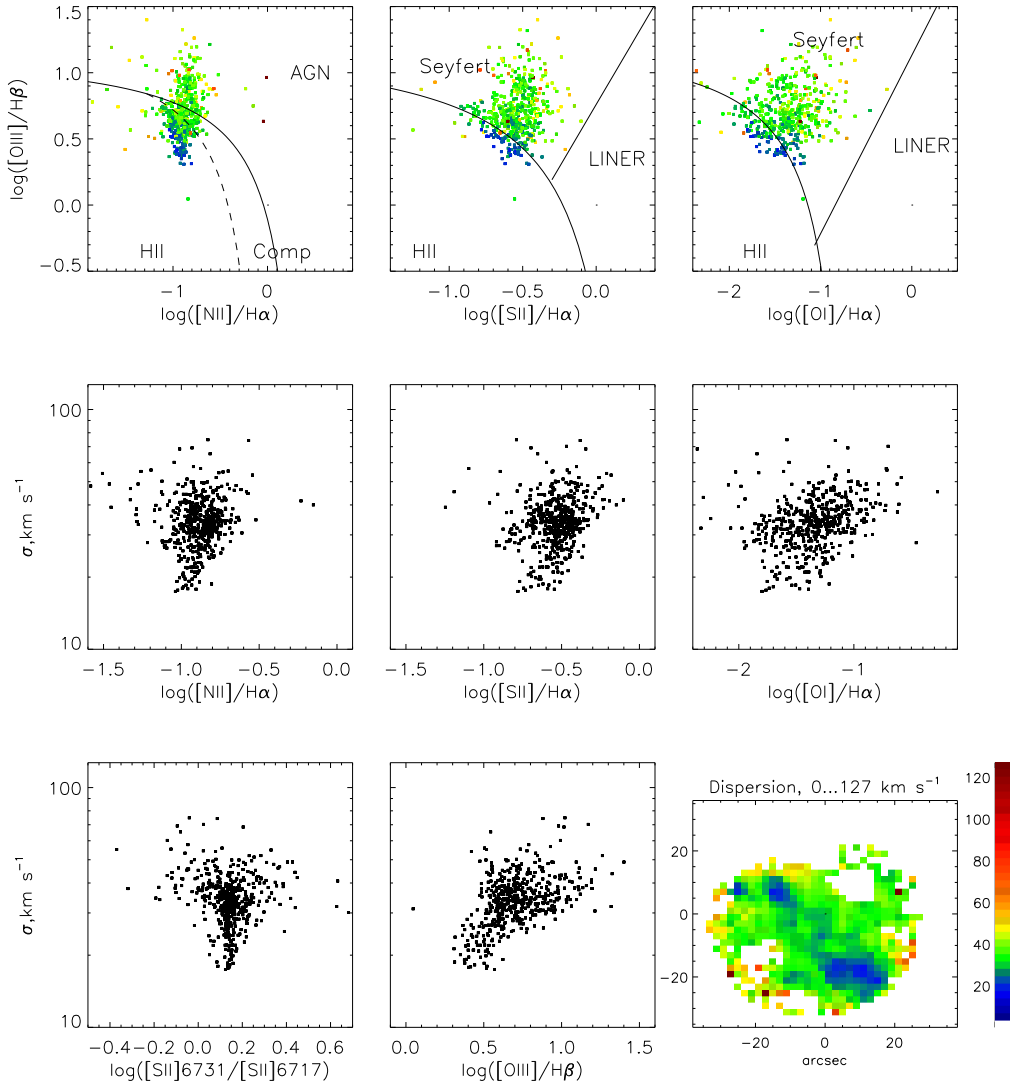


Fig. 6. Same as in Fig. 2, for Mrk 35.

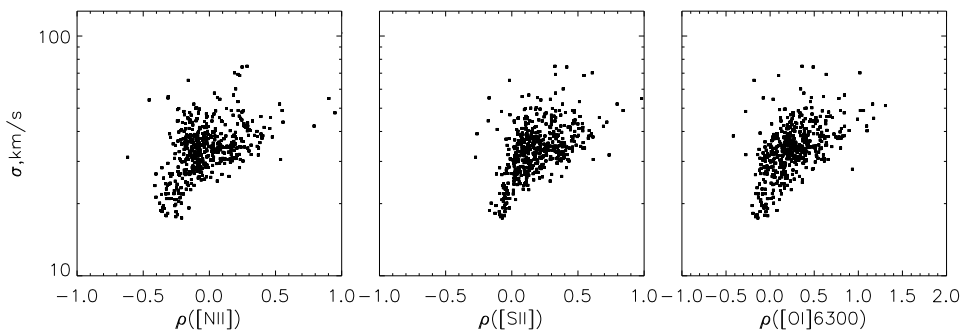


Fig. 7. Diagrams similar to those Fig. 3, for Mrk 35.

ionization in these regions. As well as in UGC 10043, the sulfur lines ratio in Fig. 6 demonstrates the anticorrelation. The σ - ρ diagrams show a positive correlation between the distance to the model curve and the velocity dispersion (Fig. 7).

3.3. Arp 212 – a Polar Ring Galaxy

Arp 212 is a peculiar galaxy in which two rotating gas subsystems that are kinematically different have been discovered: an internal disk of the 3.5-kpc size and outer H II

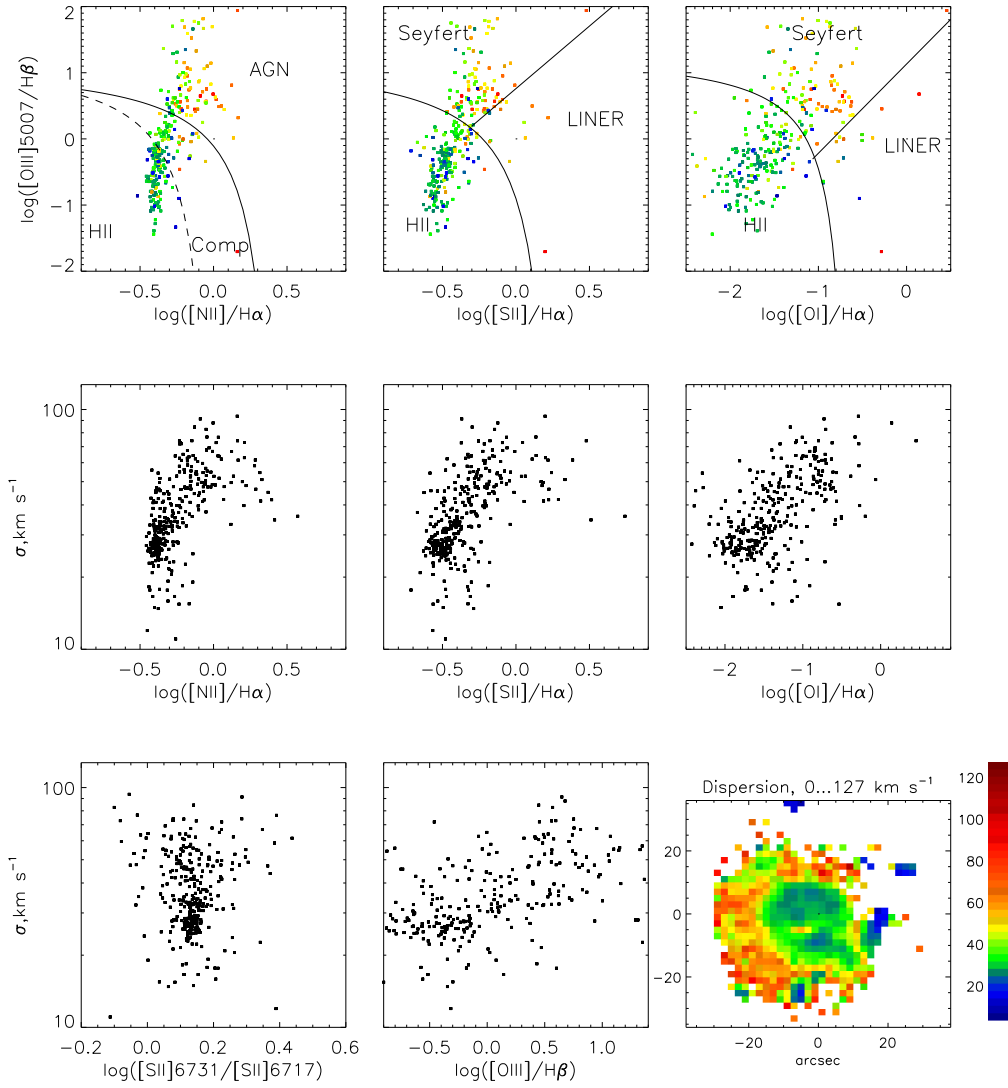


Fig. 8. Same as in Fig. 2, for Arp 212.

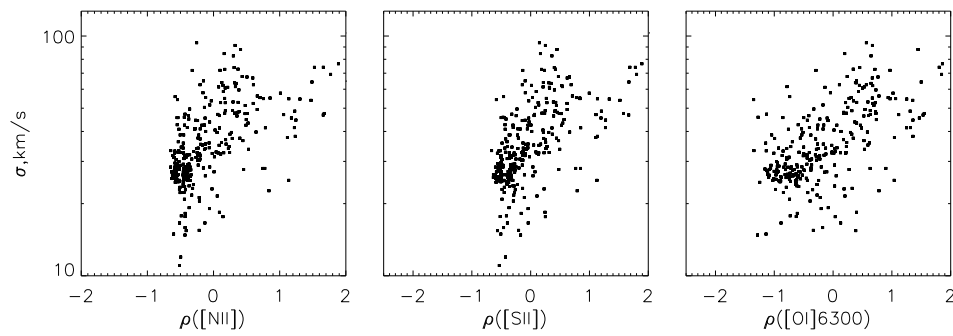


Fig. 9. Diagrams similar to those Fig. 3, for Arp 212.

regions whose orbits are inclined at a significant angle to the stellar disk (Moiseev, 2008). The observed picture was explained in the assumption that the gas (mostly neutral) in the outer regions of the galaxy is located in a wide ring of a diameter of about 20 kpc rotating in the plane almost

orthogonal to the disk. As the radii of the gaseous-cloud orbits decrease, their inclination angle decreases too; and at a radius of 2–3 kpc, the gas from the ring begins to fall out onto the plane of the galaxy inducing a burst of star formation. It is the region with the highest observed ve-

locity dispersion reaching 80–100 km s⁻¹ (see Fig. 8). The points belonging to this collision region of the gas subsystems are shifted in the BPT diagrams (Fig. 8) from the regions dominated by photoionization towards the dominance of shock ionization. At the same time, photoionization clearly dominates in the central region of the galaxy.

As well as in UGC 10043 and Mrk 35, there is a positive correlation between σ and ρ for all the BPT diagrams (Fig. 9). It is important to notice that in all three galaxies this dependence can be observed for the velocity dispersion above 30–40 km s⁻¹ and practically disappears for smaller σ . In other words, the correlation between σ and ρ manifests itself in the presence of shock excitation in the diffuse gas (DIG) and disappears in the H II regions characterized by a low level of turbulent motions. This can also be confirmed by the absence of distinct σ – ρ correlations in the galaxy VII Zw 403, where in all the points $\sigma < 40$ km s⁻¹.

As distinct from UGC 10043 and Mrk 35, the relation of sulfur lines ratio in Arp 212 does not show any pronounced dependence on σ which agrees with the assumption that high velocity dispersion is observed not only in DIG with low electron density but also in a denser medium of colliding gaseous clouds.

4. Conclusion

For an observational study of the relation between turbulent motions of the ionized gas in nearby galaxies and the state of its ionization, it is required to have panoramic spectroscopy data together with a large field of view and quite high spectral resolution. Since it is necessary to observe the low-surface-brightness region with an angular resolution of about 1'', then an optical telescope of a large ($D > 3$ –5 m) diameter is needed. All these requirements are implemented together probably only in the unique MUSE instrument at the 8-m VLT telescope (Bacon et al., 2010).

Our idea is to combine the ionization ionized gas velocity dispersion maps obtained in the observations with the scanning FPI and the panoramic spectrophotometry data for low-spectral-resolution galaxies. The observed line-of-sight velocity dispersion characterizing the turbulent motions of the ionized gas can be due to various causes such as virial motions in the galaxy's gravitational potential, the effect of expanding shells on the gas, or, more generally, energy injected into the interstellar medium by star-forming processes (see discussion and references in Moiseev et al., 2015; Krumholz & Burkhardt, 2016). Various factors influence the value of line flux relations with different excitation mechanisms. Observational information fusion makes it possible, in certain cases, to draw unambiguous conclusions about contribution of shock waves to the gas ionization in low-surface-brightness regions. From the lines flux ratio in the conical nebula in UGC 10043 only, it cannot be definitely concluded what leads the growth of the relative intensity of the forbidden lines: ionization by shock waves from the central burst of

star formation or the old stellar population of the thick disk, in which it is located. Additional information on the gas kinematics allows to say that there is a galactic wind. For Arp 212, our approach allowed to confirm the previously assumption in Moiseev (2008) on the direct collision of gaseous clouds on inclined orbits with the main disk of the galaxy generating shock fronts.

Thus, the use of the BPT– σ diagram together with the classical diagnostic methods based on lines ratios helps us better understand of ionization of the galactic interstellar medium in each specific case. The only galaxy in which we did not find a correlation between σ and characteristic line flux relations (or ρ parameter) is VII Zw 403. The ongoing star-formation rate here is the lowest in our sample ($\sim 0.015 M_{\odot} \text{yr}^{-1}$, Lozinskaya et al., 2006). Apparently, for this reason, the contribution of shock waves to gas ionization is practically invisible.

We plan to conduct further expansion of the sample of the objects under study in two ways. The first is new observations with a high spectral resolution of galaxies, for which there are the CALIFA survey data already, with the scanning FPI. The second is the creation of images in the emission lines of galaxies, for which we already have maps of the velocity dispersion of the ionized gas. Here it is proposed to use a tunable-filter photometer, the first observations with which are already being conducted by our team⁴.

Acknowledgements. The work was supported by the Russian Science Foundation (project No. 17-12-01335 “Ionized gas in galactic disks and beyond the optical radius.” The paper used the survey data provided by the Calar Alto Legacy Integral Field Area (CALIFA) survey (<http://califa.caha.es/>) based on the observations collected at the Centro Astronómico Hispano Alemán (CAHA) at Calar Alto operated jointly with the Max-Planck-Institut für Astronomie and the Instituto de Astrofísica de Andalucía (CSIC). This research has made use of the NASA/IPAC Extragalactic Database (NED) which is operated by the Jet Propulsion Laboratory, California Institute of Technology, under contract with the National Aeronautics and Space Administration. The authors are grateful to Alexandrina Smirnova and the reviewer for constructive comments.

References

- Afanasiev, V. L., Dodonov, S. N., & Moiseev, A. V. 2001, in *Stellar Dynamics: from Classic to Modern*, ed. L. P. Ossipkov & I. I. Nikiforov, 103
- Afanasiev, V. L. & Moiseev, A. V. 2005, *Astronomy Letters*, 31, 194
- Afanasiev, V. L. & Moiseev, A. V. 2011, *Baltic Astronomy*, 20, 363
- Arhipova, V. P., Lozinskaya, T. A., Moiseev, A. V., & Egorov, O. V. 2007, *Astronomy Reports*, 51, 871
- Bacon, R., Accardo, M., Adjali, L., et al. 2010, in *Proceedings of the SPIE*, Vol. 7735, *Ground-based and Airborne Instrumentation for Astronomy III*, 773508

⁴ https://www.sao.ru/Doc-en/Events/2017/Moiseev/moiseev_eng.html

- Baldwin, J. A., Phillips, M. M., & Terlevich, R. 1981, *PASP*, 93, 5
- Bundy, K., Bershady, M. A., Law, D. R., et al. 2015, *ApJ*, 798, 7
- Cairós, L. M., Caon, N., García-Lorenzo, B., et al. 2007, *ApJ*, 669, 251
- Croom, S. M., Lawrence, J. S., Bland-Hawthorn, J., et al. 2012, *MNRAS*, 421, 872
- Egorov, O. V. & Lozinskaya, T. A. 2011, *Astrophysical Bulletin*, 66, 293
- Egorov, O. V., Lozinskaya, T. A., Moiseev, A. V., & Shchekinov, Y. A. 2017, *MNRAS*, 464, 1833
- Gil de Paz, A., Madore, B. F., & Pevunova, O. 2003, *ApJS*, 147, 29
- Ho, I.-T., Kewley, L. J., Dopita, M. A., et al. 2014, *MNRAS*, 444, 3894
- Jones, A., Kauffmann, G., D'Souza, R., et al. 2017, *A&A*, 599, A141
- Kelz, A., Verheijen, M. A. W., Roth, M. M., et al. 2006, *PASP*, 118, 129
- Kewley, L. J., Dopita, M. A., Sutherland, R. S., Heisler, C. A., & Trevena, J. 2001, *ApJ*, 556, 121
- Kewley, L. J., Groves, B., Kauffmann, G., & Heckman, T. 2006, *MNRAS*, 372, 961
- Knapen, J. H., Erroz-Ferrer, S., Roa, J., et al. 2014, *A&A*, 569, A91
- Krumholz, M. R. & Burkhardt, B. 2016, *MNRAS*, 458, 1671
- López-Cobá, C., Sánchez, S. F., Moiseev, A. V., et al. 2017, *MNRAS*, 467, 4951
- Lozinskaya, T. A., Moiseev, A. V., Avdeev, V. Y., & Egorov, O. V. 2006, *Astronomy Letters*, 32, 361
- Matthews, L. D. & de Grijs, R. 2004, *AJ*, 128, 137
- Moiseev, A. V. 2008, *Astrophysical Bulletin*, 63, 201
- Moiseev, A. V. & Egorov, O. V. 2008, *Astrophysical Bulletin*, 63, 181
- Moiseev, A. V. & Lozinskaya, T. A. 2012, *MNRAS*, 423, 1831
- Moiseev, A. V., Tikhonov, A. V., & Klypin, A. 2015, *MNRAS*, 449, 3568
- Monreal-Ibero, A., Arribas, S., Colina, L., et al. 2010, *A&A*, 517, A28
- Roth, M. M., Kelz, A., Fechner, T., et al. 2005, *PASP*, 117, 620
- Sánchez, S. F., Rosales-Ortega, F. F., Kennicutt, R. C., et al. 2011, *MNRAS*, 410, 313
- Vasiliev, E. O., Moiseev, A. V., & Shchekinov, Y. A. 2015, *Baltic Astronomy*, 24, 213
- Veilleux, S. & Osterbrock, D. E. 1987, *ApJS*, 63, 295
- Zhang, K., Yan, R., Bundy, K., et al. 2017, *MNRAS*, 466, 3217